

Article

Time-of-Flight Measurements in the Jet of a High-Current Vacuum Arc Thruster

Etienne Michaux *  and Stéphane Mazouffre * 

CNRS—Institute of Combustion, Aerothermics, Reactivity et Environment (ICARE), 45071 Orléans, France

* Correspondence: etienne.michaux@cnrs-orleans.fr (E.M.); stephane.mazouffre@cnrs-orleans.fr (S.M.)

Abstract: Measurements of ion speed in the plume of a pulsed high-current vacuum arc thruster were performed by means of electrostatic probes. The probes were designed to provide direct speed measurements with minimum disturbance on the plasma jet. Typical mean values of v_i for Ti and Cu cathodes are determined at different locations downstream of the electrodes, in the far field region. From one VAT discharge to another, the mean ion speed strongly varies which leads to a large statistical dispersion. Single-shot analysis allows the observation of the plume anisotropy and its high divergence as well as the existence of several ion groups of different speeds throughout a discharge.

Keywords: vacuum arc thruster; ion speed; time of flight; pulsed discharge; high current; electrostatic probes

1. Introduction

Miniature electric propulsion devices for spacecraft have been the subject of growing interest in recent years. The gain in mass and volume electric thrusters have to offer enables lower launching costs, facilitating access to space for small companies, research institutes, universities and agencies. In this context, the vacuum arc thruster (VAT) has established itself as a technology of interest. It relies on triggering a short electrical discharge between two electrodes in a repetitive way. By doing so, the cathode material is ionized, accelerated and ejected at high speed leading to thrust generation in the opposite direction. The use of a solid metal propellant, i.e., the cathode material itself, is a key point regarding miniaturization and simplicity. In addition, as the need for a propellant tank, pipes and flow regulators is suppressed, the reliability and simplicity of these thrusters are considerably high.

However, cathodic vacuum arc plasmas are among the most difficult-to-understand uncontrolled plasma generators [1]. Despite a considerable research effort to characterize the formation and behavior of this type of plasma, few experimental data have been gathered on high-current vacuum arc discharges. Simulations have been carried out by several teams [2–4]. But the lack of experimental data is obvious, especially in the plasma jet region. The fact that the thrust level of VATs seems to be related to the arc current [5] makes such investigations therefore of interest, as recent VAT architectures tend to maximize the discharge current [6]. In order to gain a more detailed insight into the formation of the arc, its dynamics and the subsequent plasma acceleration mechanism, it is necessary to probe in depth the physics of VATs and gather data. Such a study is also necessary to propose more efficient solutions, with longer lifetimes, able to meet the requirements of a wide range of space missions.

In particular, the propellant exhaust speed is strongly related to an important thruster characteristic: the specific impulse. The specific impulse characterizes how a thruster makes an efficient use of its propellant to generate thrust. Studying the ion speed in the jet of a VAT is then of high interest. The goal of the present work is to obtain insights into the ion speed, i.e., the magnitude of the ion velocity in the measurement direction, in the jet of a high-current low-power vacuum arc thruster, namely, the plasma jet pack (PJP) thruster from the



Citation: Michaux, E.; Mazouffre, S. Time-of-Flight Measurements in the Jet of a High-Current Vacuum Arc Thruster. *Aerospace* **2023**, *10*, 1011. <https://doi.org/10.3390/aerospace10121011>

Academic Editor: Angelo Cervone

Received: 25 October 2023

Revised: 22 November 2023

Accepted: 28 November 2023

Published: 30 November 2023



Copyright: © 2023 by the authors. Licensee MDPI, Basel, Switzerland. This article is an open access article distributed under the terms and conditions of the Creative Commons Attribution (CC BY) license (<https://creativecommons.org/licenses/by/4.0/>).

COMAT company (Flourens, France). The latter is equipped with two different cathodes made out of different materials, namely titanium and copper. Preliminary measurements have already been conducted on the PJP equipped with a nickel–chromium cathode [7]. However, the experimental arrangement did not at that time allow the ion speed to be precisely determined. As the setup included a single planar probe, we assumed ions were all generated at the same moment. Thus, only the minimal ion speed was assessed. Here, a dedicated set of probes was developed to measure the ion speed at different locations in the plume without the need of any assumption on the ion generation.

This work is organized as follows. In Section 2, the thruster, methods and tools used to recover the ion speed in the plume of the VAT are presented. Section 3 proposes a commented data analysis, from a shot-to-shot comparison to a broad statistical comparison over all the measurement range. Eventually, conclusions are drawn in Section 4.

2. Thruster and Experimental Setup

2.1. PJP Thruster

The VAT under study is the Plasma Jet Pack (PJP) developed by the COMAT French company, see Figure 1a. This 30 W class VAT generates a high-current vacuum arc through the cyclic discharge of a capacitor bank. The cathode-to-anode voltage is continuously set to 250 V. A triggering system applies a pulse of a few kV on the cathode surface lasting a few hundreds of ns. This pulse allows ignition of the plasma through an explosive process occurring on a surface region named cathode spot [8]. The high voltage applied during the trigger phase initiates a breakdown by field emission [9] that is followed by a spark and then an arc. During VAT operation, a thin metallic layer deposits on the central insulator that separates the triggering system and the cathode. Ignition of the discharge is then easier as the breakdown occurs through the conductive layer. Note that when the deposited layer is thick it becomes more difficult to vaporize and the thruster no longer operates properly [10]. After the trigger is switched off, the arc is forced to propagate to the anode through the existing metal vapor. This second arc discharge allows roughly 2.5 to 4 kA to flow between the two electrodes with the present configuration, depending on the cathode material. Overall, the energy released over 30 μ s into one single PJP discharge reaches more or less 3 J. Example of a typical PJP discharge current waveform (I_d) is given in Figure 1b for titanium and copper cathodes. Despite slight differences in the maximum current from one pulse to another, the temporal evolution of the discharge current remains the same for a given cathode material. In brief the I_d waveforms are highly reproducible for a given cathode material. Measurements presented in this work have been conducted with a copper anode and two different cathode materials: titanium and copper.

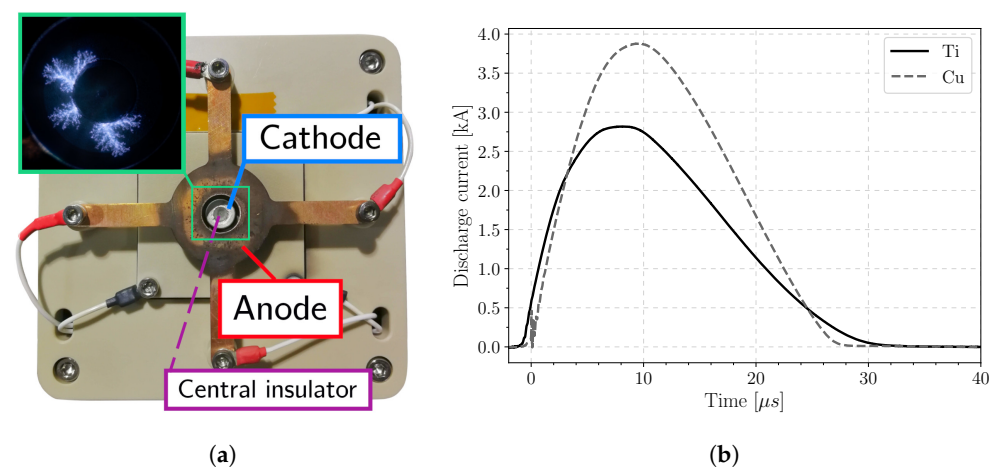


Figure 1. (a) PJP thruster: front view. In the green frame, a long-exposure photograph shows the cathode spot distribution on the PJP cathode surface during a discharge. (b) Typical PJP discharge current waveform during one pulse.

Figure 1a shows the front view of a laboratory version of the PJP. The 4-leg electrode is the annular copper anode. The cathode corresponds to the grey center-mounted hollow cylinder. The latter is screwed onto a copper plate directly wired to the capacitor bank. The gap in the axial direction between the cathode and the anode is approximately 1 cm. The trigger electrode is a tiny metal tip placed exactly on the thruster axis of symmetry and separated from the cathode with the central insulator. The picture inside the green frame in Figure 1b is a long-exposure photograph of the cathode surface during a discharge [11]. The cathode spots are here the bright branches that develop on the cathode surface. The central insulator is dark in this picture as the spots develop solely on the cathode surface. The PJP target performance and characteristics are given in Table 1 for the inclined reader.

Table 1. PJP thruster target performance and characteristics.

Power	0–30	W
Thrust to power	10	$\mu\text{N W}^{-1}$
Average thrust at 30 W	300	μN
Specific impulse	2500	s
Total impulse	400	N s
Overall mass	1	kg
Overall volume	1	U

2.2. Vacuum Chamber

Experiments were performed in the EPIC-2 vacuum facility. This tank is a stainless steel cylinder 54 cm in diameter and 104 cm in length, for an approximate capacity of 240 L. Two 2200 L/s (N_2) magnetically levitated Edwards STP-iS2207s (Edwards Vacuum, Burgess Hill, UK) are placed on top of the chamber (see Figure 2). Those pumps, evacuated through a 110 m^3/h dry primary pump (Edwards GV110), permit a background pressure of 10^{-6} mbar to be kept during thruster operation. The pressure is monitored with a Pfeiffer PBR260 Pirani/Payard-Alpert pressure gauge (Pfeiffer Vacuum, Aßlar, Germany).

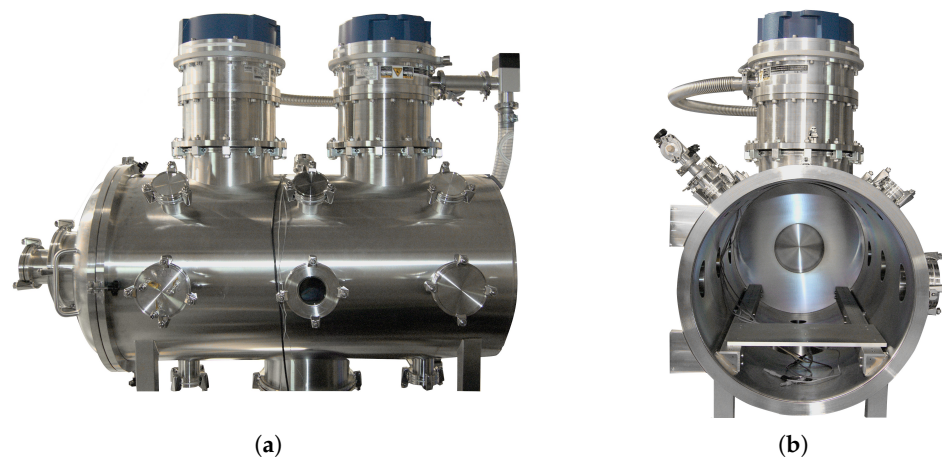


Figure 2. Photographs of the EPIC-2 vacuum chamber. The two STP-iS2207s are seen on the top of the chamber. (a) Side view. The door of the tank is on the left, a glass window is seen in the center of the picture. (b) Inside view of the chamber, through the open door. The rails and the thruster support plate are here placed inside.

EPIC-2 is also equipped with several electrical feedthroughs, for both in situ diagnostics and thruster power supply. Those feedthroughs are mostly composed of BNC or SubD connectors. Two Kodial (Borosilicate 7056) glass windows allow the visual inspection of the thruster during operation.

In EPIC 2, the PJP is mounted on a square fixed to a plate, the latter being screwed on rails. This mounting allows adjustments of the distance to the windows or to instruments,

depending on the experiment to be performed. For investigating the plasma plume by means of electrostatic probes, the PJP is placed far back in the tank to let the plume expand as freely as possible.

2.3. Time-of-Flight Technique

Time of flight is in short the measurement of the time taken by a particle to travel a given distance. Here, particles are ions and the medium is a plasma. Assuming that the ion trajectory is a straight line, this method consists of measuring the ion current simultaneously at 2 different locations with probes. As the plasma is here pulsed, the collected current rises up and then falls back to zero. Recorded signals are in fact not smooth with well identified structures. The time difference Δt between those structures gives the ion speed. Note (see Figure 3b) that although ion current waveforms are complicated, the overall shape does not vary much from one pulse to another with reproducible features. To ensure the accuracy of this method, probes should first be negatively polarized to solely capture ions. In this study the bias voltage is set to -35 V, which is enough to repel the overwhelming majority of electrons in the plasma jet [7]. Note that the probes should be equally biased to avoid the presence of an electric field in between. They must also be far from each other for their plasma sheaths not to interact. Ultimately, the first probe that the plasma jet encounters should disrupt the flow as little as possible. In that respect, a ring-shaped probe (RP) was developed. This probe consists of a 15 mm diameter loop formed with a 0.6 mm in diameter tungsten wire. This geometry allows ions to be collected without disturbing the central cone of the plasma jet. Further downstream ions are collected by a 6 mm in diameter planar probe (PP). The choice of making the RP diameter more than two times bigger than the PP diameter is to ensure that the ring does not screen the planar probe. In this regard, this setup is improved compared to the one previously developed [12] of which the first probe was a grid, therefore disturbing the plasma flow. Probes are positioned 4 cm apart and placed at different positions in the plasma plume of the VAT as explained in the next sections. A photograph of the set of probes is presented in Figure 3a.

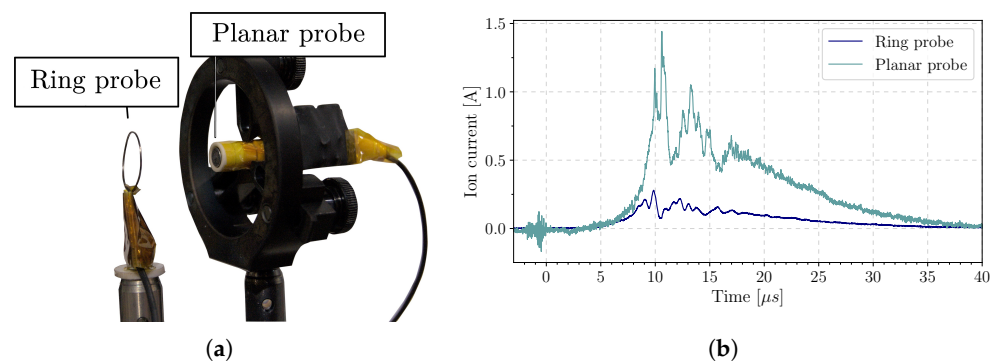


Figure 3. Time-of-flight probes and typical traces. (a) Time-of-flight (ToF) probe arrangement. (b) Example of ion current waveform recovered by the two ToF probes during one pulse (Ti, 23 cm from anode, on axis).

It is particularly important in that experiment that the current probes used to measure the current flowing through the electrostatic probes are strictly similar. This is the reason why two calibrated 50Ω Pearson 2878 current transformers (Pearson Electronics Inc., Palo Alto, CA, USA) are placed in the circuit to monitor the evolution in time of the ion current. They can measure a maximum current of 400 A and their bandwidth spread is from 10 Hz to 70 MHz, which is sufficient to recover the structures of interest in the ion current waveforms. The power supply used to bias both the ring probes and the planar probes was a Tenma 72-10480 (Farnell, Leeds, UK). A schematic of the experimental setup is presented in Figure 4. Figure 3b shows an example of ion current waveforms recorded with the ToF setup with a Ti cathode. As previously explained, signals are complex with well defined peaks visible

on the two traces. The difference in amplitude is due to the difference in the two ToF probe collection areas.

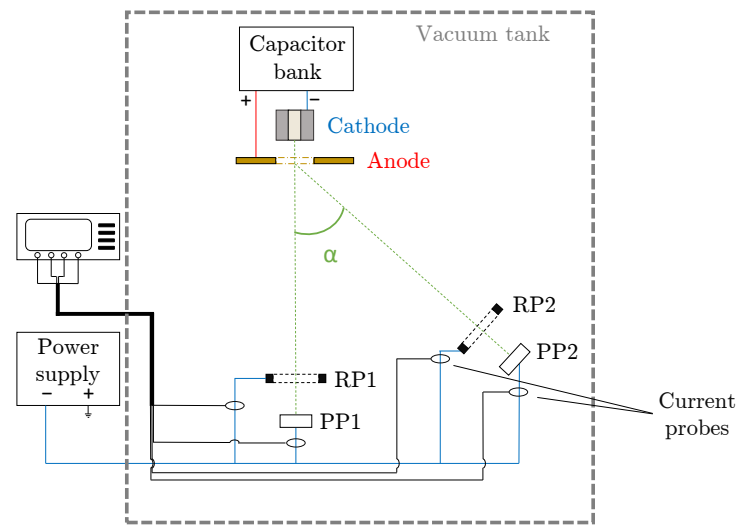


Figure 4. Layout of the experimental setup for measuring the ion speed in the plasma jet of the PJP with the ToF technique. Arc triggering system not represented. Not to scale.

3. Ion Speed

3.1. Far Downstream

At first, a cross-correlation analysis between the RP and the PP signals was considered to retrieve the ion speed. However, the first results showed (see Figure 3b) that the two waveforms are not strictly similar, leading to inaccuracy while using cross-correlation. Therefore, a more favorable approach is to identify the different peaks and determine their respective speeds. In other words, it is necessary not to process the waveform as a whole but to separately analyze its components in order to obtain an accurate representation of the speed distribution [12]. As can be seen in Figure 3b, traces are quite noisy and exhibit many peaks. To ease peak identification, the signals are filtered through a 1 MHz cutoff frequency low-pass filter. Then, a normalization in magnitude is carried out to ease the comparison. Eventually, the peaks are identified with a custom-built algorithm. The different peaks are identified on the RP waveform according to fixed conditions: minimal amplitude, width, time between the different peaks and prominence, i.e., relative amplitude with respect to the surroundings. An array containing the time of occurrence and the amplitude of all peaks is created. Peaks with similar amplitude are then sought in the PP waveform, within a range defined by the cross-correlation time shift. Carrying that out, the results are more precise when it comes to identifying the same peak on the RP and the PP. If no corresponding peak is found on the PP waveform, or if the shape of the peak is too different, the ToF is not calculated.

The result of the peak identification procedure is shown in Figure 5. The time $t = 0$ refers to the moment the oscilloscope is triggered, when the discharge current reaches 500 A. This value is set to avoid recording the electromagnetic noise associated with the activation of the PJP high-voltage trigger. The amplitude of this noise can exceed the maximum value of ion current I_i at the probes, which induces an error while normalizing the waveform.

Although the waveforms recovered from the ToF probes slightly vary from one PJP discharge to another, the appearance of at least two peaks is systematically observed. In this study, we focus on the three main peaks that emerge from the ion current waveform, the third one being sometimes missing. These peaks are different ion populations, generated at different times during the discharge. The vacuum arc appears to move across the cathode surface and this apparent motion takes place via local micro-explosions [13]. The different peaks may result from the ionization of larger volumes from the cathode material, in the

course of the vacuum arc motion. The possibility that these peaks are ion populations with different charges cannot be ruled out either, although it is more unlikely. In the case of a purely electrostatic acceleration, assuming that ions are created at the same time, the ratio between speeds should be approximately equal to the ratio between charges, which is not seen here, as we will see later. Multiply charged ions exist in large quantities in vacuum arcs [14,15]. Here, it seems more likely that ions with different charges are created all throughout the discharge. With this assumption, ions with a higher charge state generated at the end of the discharge would strike the probes at the same moment as slower ions created earlier, making the precise identification of the charge impossible with the current method. The peaks observed in Figures 5 and 6 are not solely due to a difference in charge, then. Thus, the exact contribution of each physical mechanism leading to their observation remains uncertain.

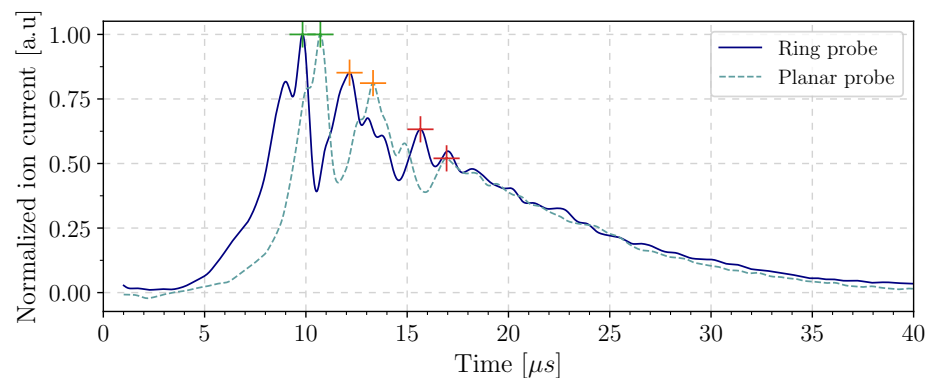


Figure 5. Filtered and normalized ToF traces from Figure 3b. Colored crosses indicate the 3 main populations accounted for in the speed calculation.

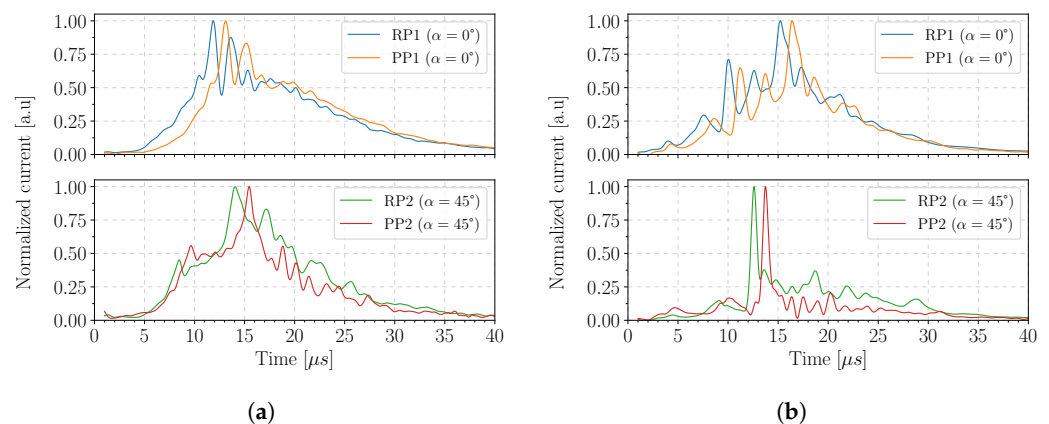


Figure 6. On- and off-axis ion traces (single shot) for a Ti and a Cu cathode. (a) Titanium. (b) Copper.

In Figure 5, the first identified population is indicated in green and presents a speed of 45 km/s. Then, the second population (orange) shows a 34 km/s speed whereas the third one (red) reveals the lowest speed, about 31 km/s. Hereafter in the study, the first, second and third peaks refers to the respective times of occurrence and not to the magnitude in ion current. This example is highly representative of the current waveforms we acquired in the VAT plasma. In short, the first ion group, or population, is faster than the second, the latter being in turn faster than the third one.

Figure 7 shows a histogram of the speed distribution of the different populations, over 100 discharges performed with Figure 7a a titanium cathode and Figure 7b a copper cathode. The ToF probes were placed 23 cm downstream of the anode (anode–RP distance). The mean speed for each population is given in Tables 2 and 3. The probability density function is plotted for each ion population to ease visualization. Distributions can rea-

sonably be represented by a Gaussian function. Titanium ion speed ranges from 17 km/s to almost 50 km/s, whereas copper ion speed ranges from 13 km/s to 50 km/s which is higher than what is usually found in the literature [16]. This high ion speed in the plume of the PJP has already been noted with a nickel–chromium cathode [7].

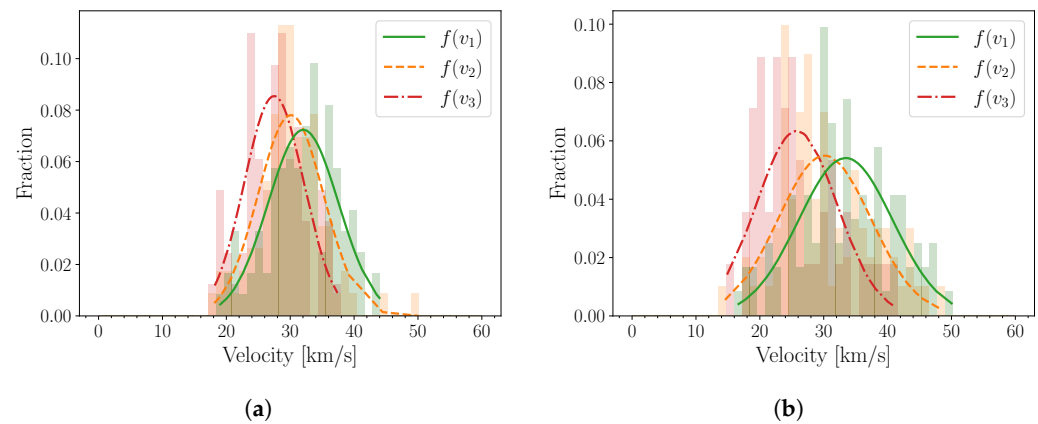


Figure 7. Ion speed distribution, 23 cm away from the anode. (a) Titanium cathode. (b) Copper cathode.

This can be explained by the fact that the discharge current is here much higher than in most experimental arrangements set to study vacuum arcs. The energy released by the capacitors in the circuit, and thus into the plasma, is here of several joules. The correlation between the increase in discharge current and the increase in the ion speed has already been observed for lower current vacuum arcs in ref. [17]. Concerning the ordering of the population depending on their speed, it is noted that the first peak appearing in the waveform is the fastest on average. Assuming ions are created throughout the discharge, peaks occurring at the beginning of the discharge are faster than the ones appearing in the middle, although the maximum in discharge current I_d is not yet reached. This ordering is observed in the overwhelming majority of the discharges. A few exceptions can be found for some pulses. For example, in Figure 7a the fastest ions are around 50 km/s and they correspond to the second population that appears during the discharge.

3.2. Influence of the Ejection Angle

Studying the ion speed as a function of the ejection angle with respect to the plasma jet axis provides information on the homogeneity of the plume and on the way the plasma expands. Two similar arrays of ToF probes were then placed on-axis and off-axis at different angles from the centerline. Measurements presented in this section are taken 20 cm away from the cathode center. Following the method presented in the previous section, examples of titanium and copper ion current waveforms are plotted in Figure 6.

Waveforms recorded at larger angles show several peaks but their occurrence in time is different compared with on-axis measurements. In Figure 6a, for the titanium cathode, the ion population appears first on the set of probes placed at 45° and then appears on-axis. In the example shown in Figure 6b, where the PJP is equipped with a copper cathode, the situation is reversed. Measurements at 45° show a single main peak, whereas many peaks and a broad profile are observed on-axis. Overall, ion current waveforms recorded off-axis show similar properties with respect to the on-axis waveforms: the typical duration is about $40 \mu\text{s}$ and several peaks are observed. The occurrence in time of those peaks varies significantly from one pulse to another. Moreover, in the course of a given discharge I_i waveforms are never the same depending on the observation location. In particular, see Figure 6, the maximum in ion current is not reached at the same moment for the two sets of probes, even though they are at the same distance from the anode. This demonstrates the anisotropy of the plume.

Measurements at larger angles, see Figure 8, present the same pattern. From time to time, ions are even faster 60° from the centerline than on-axis. It is, however, noted that

quite frequently the plasma does not reach the probes placed at 60° whereas the signal is measured on the axis. This shows the high divergence of the plasma jet. It also indicates that the ejection direction is not the same depending on the pulse, that direction being therefore not aligned with the thruster centerline. The explanation lies in the circular shape of the cathode exposed surface. The latter has a disk-shaped surface that allows the cathode spots to develop radially. It was observed in ref. [11] that the spots do not cover the entire cathode surface during a pulse, as they tend to develop in branches that are not symmetrical relative to the disk center. This certainly leads to some directivity when ejecting the cathode material in the form of a plasma.

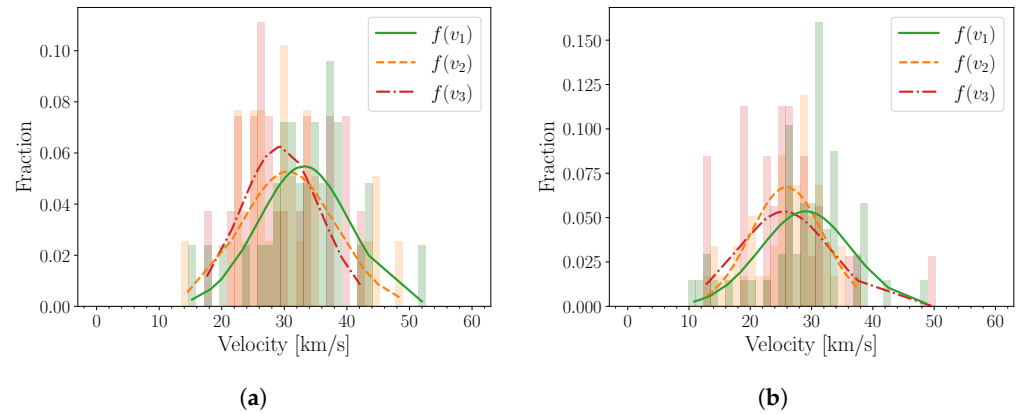


Figure 8. Ti ion speed distribution 20 cm from the anode plane for different angles: (a) 45° dataset; (b) 60° dataset.

3.3. Evolution along the Centerline

The ToF probe array has been moved along the PJP centerline to examine the change in the ion speed with the distance to the thruster. Measurements cover the [9–32] cm range. Below 9 cm, the ion current density in the jet was too high thus saturating the probes. This made data acquisition impossible with the current ToF setup, despite the very small ion collection area. Hence, the PJP plume near-field region has not been investigated in this study. Beyond 32 cm the study was not continued as no significant evolution was observed along the axis, as shown in Figures 9 and 10.

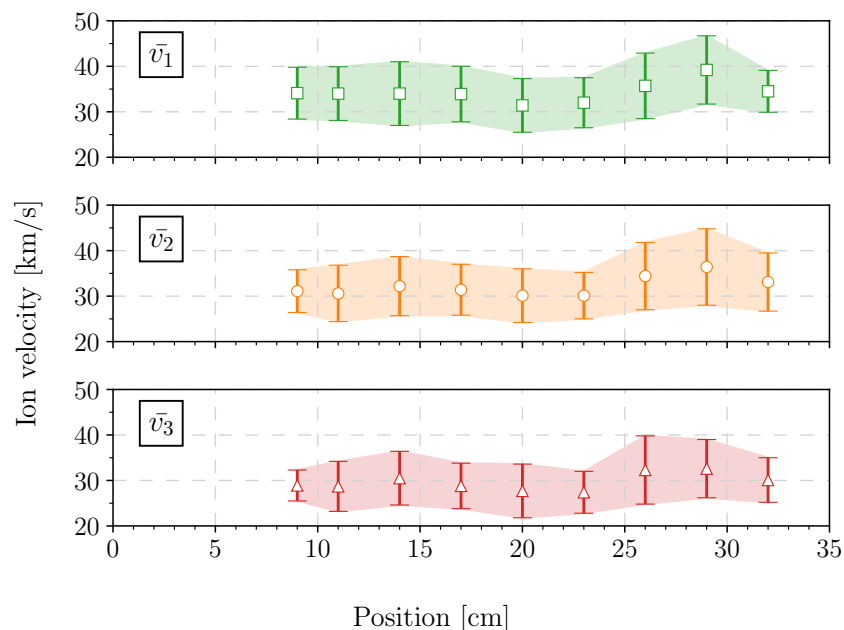


Figure 9. Mean Ti ion speed along the VAT plasma jet axis. The subscript refers to the ion population.

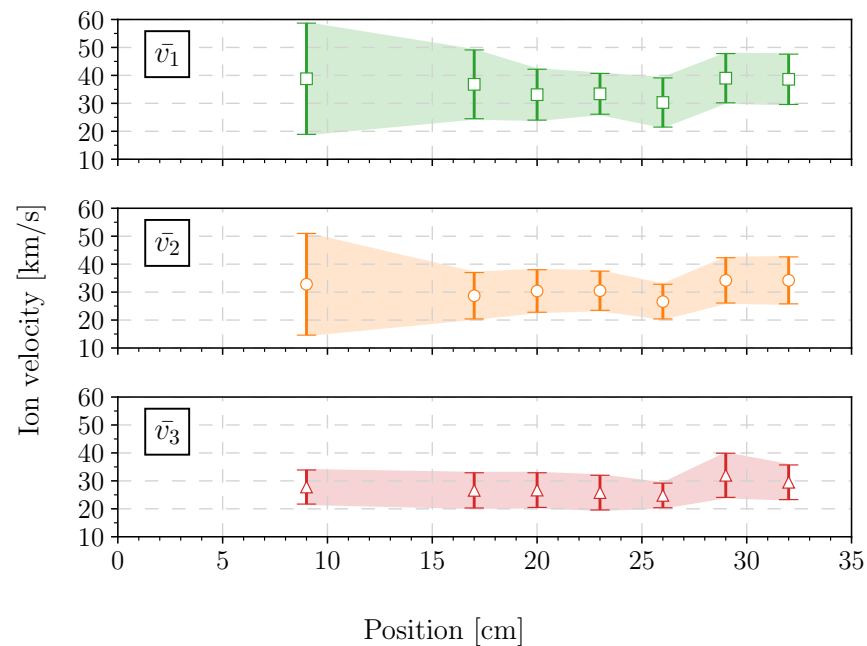


Figure 10. Mean Cu ion speed along the VAT plasma jet axis. The subscript refers to the ion population.

Figure 9 shows the evolution of the titanium ion mean speed, as well as the associated standard deviation for each position. \bar{v}_1 , \bar{v}_2 and \bar{v}_3 represent, respectively, the mean speeds of the first, second and third populations in the waveform, as exemplified in Figures 5 and 7. A similar graph has been plotted for copper ions in Figure 10. Two points ($x = 11$ cm, $x = 14$ cm) have been removed due to an issue with thruster operation while equipped with the copper cathode. Numerical data are given in Tables 2 and 3 for the two materials for the inclined reader.

Table 2. Values of mean Ti ion speeds.

Distance [cm]	v_1 [km/s]	v_2 [km/s]	v_3 [km/s]
9	34.1	31.1	28.9
11	34.0	30.6	28.7
14	34.0	32.2	30.5
17	33.9	31.4	28.8
20	31.4	30.1	27.7
23	32.0	30.1	27.4
26	35.7	34.4	32.3
29	39.2	36.4	32.6
32	34.5	33.1	30.1

Table 3. Values of mean Cu ion speeds.

Distance [cm]	v_1 [km/s]	v_2 [km/s]	v_3 [km/s]
9	38.8	32.8	27.8
17	36.8	28.7	26.6
20	33.1	30.4	26.7
23	33.4	30.5	25.8
26	30.3	26.6	24.8
29	39.0	34.2	32.0
32	38.6	34.1	39.5

\bar{v}_1 for titanium varies from 31 to 39 km/s with a standard deviation between 5.6 and 7.5 km/s. The rather high standard deviation exemplifies the uniqueness of each arc, making it necessary to acquire data over a very large number of pulses to extract a global behavior. Moreover, a higher statistical dispersion is remarked for copper, despite \bar{v}_1 being quite similar in terms of magnitude, which is consistent with previous studies [18,19]. Note that the large dispersion at 9 cm is due to the observation of very fast ion populations. This phenomenon is discussed in the next section. These speed measurements correspond to a mean kinetic energy ranging from 214 to 286 eV in case of titanium ions, whereas the copper ion kinetic energy ranges from 250 to 417 eV. These values are much higher than in other works [16,18,20,21] which is not so surprising as both the discharge current intensity and its growth rate $\dot{I} = dI/dt$ are orders of magnitude higher here. As previously mentioned, a correlation between the increase in discharge current and the increase in ion velocity has already been referenced [17]. It can be added that a high current growth rate [22] leads to a higher ion energy. This last effect explains why copper ions are as fast as titanium ions with our experimental conditions, see Figure 1b, despite the fact that they are heavier. On the other hand, one can notice once again that the first population is on average faster than the second, itself faster than the third one. The change in \dot{I} is surely the main driver in this observation but another phenomenon comes into play. As the discharge lasts, metal evaporation from macroparticles and vanishing cathode spots fill the inter-electrode gap with neutrals and reduce the ion mean charge [14,17]. This naturally leads to a decrease in the mean ion velocity. Moreover, as the capacitor bank discharges, the voltage drops between the cathode and the anode [20]. The external electric field is then gradually reduced and ions experience less electrostatic acceleration.

Finally, no significant spatial evolution of the ion speed is observed in the probed region. This indicates that the acceleration process takes place close to the cathode–anode region, which is consistent with previous studies [16,18,20,21,23,24]. It is therefore of interest to probe the near-field region, closer to the electrodes, to investigate the nature of plasma acceleration mechanisms.

3.4. Fast Ions

In this study, a total of 16,000 traces were analyzed. Among them, one Ti population and four Cu populations show a speed higher than 80 km/s. These fast populations have subsequently a very low probability of occurrence. Figure 11 shows the fastest population recorded with the ToF setup over the whole dataset. The measured speed reaches 160 km/s for Cu ions which corresponds to a specific impulse of 16,310 s. As a comparison, the highest measured speed for the Ti ion dataset is 85 km/s.

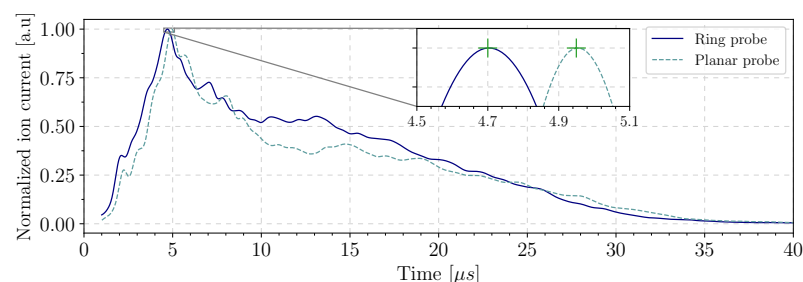


Figure 11. ToF traces showing the fastest ion population observed. Cu cathode 9 cm away from the anode.

Those fast ions are surely multiply charged ions, that are known to be produced in large numbers in vacuum arc discharges [3,15,25–28]. By definition, these multiply charged ions are subject to a higher electrostatic or electromagnetic acceleration in the inter-electrode gap. As can be seen in Figure 11, according to the population speed and the occurrence time, these ions are created during the steady state arc regime and not during the spark [7,15]. Their presence may be due to a sausage-type instability leading to local micro pinches that

heat the plasma [29,30]. These kinds of instability need a high current to arise and could explain why the apparition of this fast population occurs when the discharge current is almost at its maximum.

4. Conclusions

The ion speed in the jet of a high-current vacuum arc thruster was assessed using the time-of-flight method. Ion populations with different speeds were observed during a single pulse. In the vast majority of the observations, the earlier a population appears during the discharge the faster it is, meaning that the maximum ion speed is reached before the maximum in discharge current. The main driver in this observation is the I_d growth rate.

The thruster was equipped with a titanium and a copper cathode. On average, copper ions are more energetic than titanium ions with a mean kinetic energy of 327 eV against 252 eV when accounting for the three main ion groups. Mean speeds do not significantly change along the thruster centerline, as the acceleration zone is upstream of the measured range, in the vicinity of the cathode surface (less than 1 mm). Also, little difference in the mean ion speed is noticed on axis and off axis. It is, however, observed that, for a given discharge, ion current waveforms remarkably vary depending on the measuring location in the plume. This demonstrates that the plasma jet of a VAT is highly heterogeneous and presents a high divergence.

From one discharge to another, ion speeds are significantly different which results in a large statistical dispersion. A copper ion population with a speed of 160 km/s has even been recorded, surely due to the presence of high current plasma instabilities. This unique nature of each vacuum arc discharge is quite problematic when it comes to characterizing VAT performances and can lead to uncertainties for some precision maneuvers in space. Despite that, this high ejection speed is a positive point as it correlates with the specific impulse of the thruster. Measurements performed in this study indicate that the ion speed in the jet of a high-current VAT is higher than in most electric propulsion technologies [31]. Complementary thrust measurement would be of interest to investigate correlations between the plasma behavior and the overall VAT performance.

Author Contributions: Conceptualization, E.M. and S.M.; methodology, E.M.; validation, S.M.; investigation, E.M.; writing—original draft preparation, E.M. and S.M.; writing—review and editing, E.M. and S.M.; visualization, E.M.; supervision, S.M.; funding acquisition, S.M. All authors have read and agreed to the published version of the manuscript.

Funding: E.M. benefits from a CNES-COMAT Ph.D. grant.

Data Availability Statement: Not applicable.

Conflicts of Interest: The authors declare no conflict of interest.

References

1. Anders, A. The evolution of ion charge states in cathodic vacuum arc plasmas: A review. *Plasma Sources Sci. Technol.* **2012**, *21*, 035014. [[CrossRef](#)]
2. Chapelle, P.; Bellot, J.; Duval, H.; Jardy, A.; Ablitzer, D. Modelling of plasma generation and expansion in a vacuum arc: Application to the vacuum arc remelting process. *J. Phys. D Appl. Phys.* **2001**, *35*, 137. [[CrossRef](#)]
3. Garrigues, L.; Sarrailh, P. Generation of multiply charged ions in the context of a vacuum arc thruster. In Proceedings of the 37th International Electric Propulsion Conference (IEPC 2022), Boston, MA, USA, 19–23 June 2022; p. 519.
4. Delachaux, T.; Fritz, O.; Gentsch, D.; Schade, E.; Shmelev, D.L. Numerical simulation of a moving high-current vacuum arc driven by a transverse magnetic field (TMF). *IEEE Trans. Plasma Sci.* **2007**, *35*, 905–911. [[CrossRef](#)]
5. Kühn, M.; Tournel, C.; Schein, J. Thrust Measurements on the High Efficient and Reliable Vacuum Arc Thruster (HERVAT). *Appl. Sci.* **2021**, *11*, 2274. [[CrossRef](#)]
6. Blanchet, A.; Herrero, L.; Voisin, L.; Pilloy, B.; Courteville, D. Plasma Jet Pack Technology for Nano-Microsatellites. In Proceedings of the 36th International Electric Propulsion Conference, Vienna, Austria, 15–20 September 2019.
7. Michaux, E.; Mazouffre, S.; Blanchet, A. Time evolution of plasma parameters in the jet of a low-power vacuum arc thruster. *J. Electr. Propuls.* **2022**, *1*, 7. [[CrossRef](#)]
8. Mesyats, G. Ecton or electron avalanche from metal. *Physics-Uspeski* **1995**, *38*, 567. [[CrossRef](#)]

9. Alpert, D.; Lee, D.; Lyman, E.; Tomaschke, H. Initiation of electrical breakdown in ultrahigh vacuum. *J. Vac. Sci. Technol.* **1964**, *1*, 35–50. [[CrossRef](#)]
10. Keidar, M.; Schein, J.; Wilson, K.; Gerhan, A.; Au, M.; Tang, B.; Idzkowski, L.; Krishnan, M.; Beilis, I. Magnetically enhanced vacuum arc thruster. *Plasma Sources Sci. Technol.* **2005**, *14*, 661. [[CrossRef](#)]
11. Michaux, E.; Vinci, A.; Mazouffre, S. Fractal dimension of cathode spots in a high-current vacuum arc thruster. *Vacuum* **2023**, *215*, 112286. [[CrossRef](#)]
12. Michaux, E.; Mazouffre, S.; Fritzsche, R. Spatial and temporal evolution of ion and electron parameters in the plasma jet of a 30W VAT. In Proceedings of the 37th International Electric Propulsion Conference, Boston, MA, USA, 19–23 June 2022.
13. Siemroth, P.; Schulke, T.; Witke, T. Investigation of cathode spots and plasma formation of vacuum arcs by high speed microscopy and spectroscopy. *IEEE Trans. Plasma Sci.* **1997**, *25*, 571–579. [[CrossRef](#)]
14. Anders, A.; Oks, E.; Yushkov, G. Production of neutrals and their effects on the ion charge states in cathodic vacuum arc plasmas. *J. Appl. Phys.* **2007**, *102*, 043303. [[CrossRef](#)]
15. Yushkov, G.; Anders, A. Extractable, elevated ion charge states in the transition regime from vacuum sparks to high current vacuum arcs. *Appl. Phys. Lett.* **2008**, *92*, 041502. [[CrossRef](#)]
16. Yushkov, G.; Anders, A.; Oks, E.; Brown, I. Ion velocities in vacuum arc plasmas. *J. Appl. Phys.* **2000**, *88*, 5618–5622. [[CrossRef](#)]
17. Hohenbild, S.; Grübel, C.; Yushkov, G.; Oks, E.; Anders, A. A study of vacuum arc ion velocities using a linear set of probes. *J. Phys. D Appl. Phys.* **2008**, *41*, 205210. [[CrossRef](#)]
18. Byon, E.; Anders, A. Ion energy distribution functions of vacuum arc plasmas. *J. Appl. Phys.* **2003**, *93*, 1899–1906. [[CrossRef](#)]
19. Anders, A.; Yushkov, G.Y. Angularly resolved measurements of ion energy of vacuum arc plasmas. *Appl. Phys. Lett.* **2002**, *80*, 2457–2459. [[CrossRef](#)]
20. Beilis, I. *Plasma and Spot Phenomena in Electrical Arcs*; Springer Nature: Berlin/Heidelberg, Germany, 2020; Volume 113. [[CrossRef](#)]
21. Barengolts, S.; Mesyats, G.; Shmelev, D. Mechanism of ion flow generation in vacuum arcs. *J. Exp. Theor. Phys.* **2001**, *93*, 1065–1073. [[CrossRef](#)]
22. Astrakhantsev, N.; Krasov, V.; Paperny, V. Ion acceleration in a pulse vacuum discharge. *J. Phys. D Appl. Phys.* **1995**, *28*, 2514. [[CrossRef](#)]
23. Hantzsche, E. Mysteries of the arc cathode spot: A retrospective glance. *IEEE Trans. Plasma Sci.* **2003**, *31*, 799–808. [[CrossRef](#)]
24. Hantzsche, E. Two-dimensional models of expanding vacuum arc plasmas. *IEEE Trans. Plasma Sci.* **1995**, *23*, 893–898. [[CrossRef](#)]
25. Yushkov, G.; Anders, A.; Frolova, V.; Nikolaev, A.; Oks, E.; Vodopyanov, A. Plasma of vacuum discharges: The pursuit of elevating metal ion charge states, including a recent record of producing Bi¹³⁺. *IEEE Trans. Plasma Sci.* **2015**, *43*, 2310–2317. [[CrossRef](#)]
26. Koshelev, K.; Pereira, N. Plasma points and radiative collapse in vacuum sparks. *J. Appl. Phys.* **1991**, *69*, R21–R44. [[CrossRef](#)]
27. Yushkov, G.; Nikolaev, A.; Frolova, V.; Oks, E.; Roussikh, A.; Zhigalin, A. Multiply charged metal ions in high current pulsed vacuum arcs. *Phys. Plasmas* **2017**, *24*. [[CrossRef](#)]
28. Nikolaev, A.G.; Yushkov, G.Y.; Savkin, K.P.; Oks, E.M. Angular distribution of ions in a vacuum arc plasma with single-element and composite cathodes. *IEEE Trans. Plasma Sci.* **2013**, *41*, 1923–1928. [[CrossRef](#)]
29. Romanov, I.; Tsygvintsev, I.; Paperny, V.; Kologrivov, A.; Korobkin, Y.V.; Krukovskiy, A.Y.; Rupasov, A. Influence of the laser plasma-expansion specific on a cathode jet formation and the current stability in a laser-ignited vacuum discharge. *Phys. Plasmas* **2018**, *25*, 083107. [[CrossRef](#)]
30. Romanov, I.; Paperny, V.; Korobkin, Y.V.; Podviaznikov, V.; Rupasov, A.; Chevokov, V.; Shikanov, A. Observation of micropinch formation in cathode jet of a low-power laser-induced vacuum discharge. *Phys. Plasmas* **2016**, *23*, 023112. [[CrossRef](#)]
31. Mazouffre, S. Electric propulsion for satellites and spacecraft: Established technologies and novel approaches. *Plasma Sources Sci. Technol.* **2016**, *25*, 033002. [[CrossRef](#)]

Disclaimer/Publisher’s Note: The statements, opinions and data contained in all publications are solely those of the individual author(s) and contributor(s) and not of MDPI and/or the editor(s). MDPI and/or the editor(s) disclaim responsibility for any injury to people or property resulting from any ideas, methods, instructions or products referred to in the content.